Optical Force Sensor Based on Whispering Gallery Mode Resonators

Michael Kozhevnikov, [*] Tindaro Ioppolo.[†], Vadim Stepaniuk.[‡], Valery Sheverev [§] and Volkan Otugen[**]

Polytechnic University, Brooklyn, NY 11201

This paper discusses a novel micro-optical force sensor based on dielectric microspheres that are excited by coupling light from optical fibers. The technique exploits the morphology-dependent shifts in resonant frequencies that are commonly referred to as the whispering gallery modes (WGM). A small change in the size, shape or optical constants of the microsphere causes a shift in the resonant frequency (or the WGM). For example, a compression force applied to the microsphere will lead to a change in both its shape and its index of refraction distribution. These changes will result in a shift of the WGM. By monitoring this shift, the magnitude of the applied force can be determined. The WGM shifts are observed by scanning a tunable diode laser that is coupled into the optical fiber on one end and monitoring the transmission spectrum by a photo diode on the other end. When the microsphere is in contact with a bare section of the fiber, the optical modes are observed as dips (due to destructive interference) in the intensity of the light transmitted through the fiber. Current results demonstrate the WGM shifts due to compression force applied to micro-spheres along the polar direction. The measurements also indicate a force measurement resolution of $\sim 10^{-2}$ N with the current sensor design.

I. Introduction

OPTICAL micro-sphere resonators have attracted interest due to their unique properties including the very high quality factor (Q-factor) they can exhibit. The quality factor, $Q = \lambda/\Delta\lambda$ (λ is the wavelength of the laser), is a measure of how well an optical resonance (or WGM) of the sphere is resolved. Q-factors as high as 10^9 have been reported in the literature.[1] The very high values of Q allow for the determination of very small morphology dependent shifts in WGMs of the optical sphere.

The morphological changes (such as the size, shape or the index of refraction of the sphere) can be caused by a change in the physical condition of the surrounding. Recently, several applications of optical microspheres have been explored including temperature sensing[2] and protein detection.[3-5] In the present, we demonstrate the optical micro-sphere as a force sensor. The measurement principle is based on mode shifts of dielectric micro-resonators and exploits recent developments in optical fiber and switching technologies. The sensing element, typically a microsphere with a diameter of 200 to 300 μm, is weakly coupled to an optical fiber as shown in Fig. 1. The optical fiber, which carries light from a tunable laser, serves as an input/output port for the microsphere. When the microsphere is coupled to an exposed section of the fiber core (see Fig. 2), its optical resonances are observed as sharp dips in the transmission spectrum as shown in Fig. 3. These optical resonances (WGM), are extremely narrow and highly sensitive to changes in the refractive index as well as the shape and size of the sphere. A minute change in any of these properties of the sphere causes shifts of the resonance positions allowing for the precise measurement of the temperature, pressure or force that is responsible for the change.

[*] Present Affiliation: Scientist, Lenterra, Inc. Newark, NJ 07102.
[†] Graduate Research Assistant, Mechanical & Aerospace Engineering, AIAA Student Member.
[‡] Graduate Research Assistant, Mechanical & Aerospace Engineering, AIAA Student Member.
[§] Industry Associate Professor, Physics,
[**] Professor, Mechanical & Aerospace Engineering, AIAA Associate Fellow.

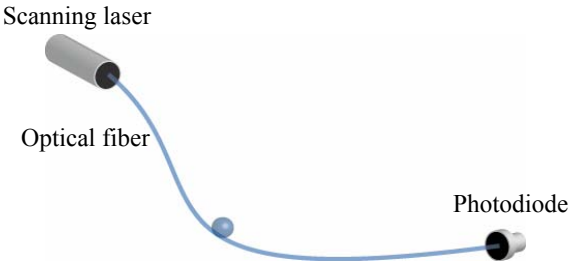

Figure 1: Schematic representation of WGM sensor

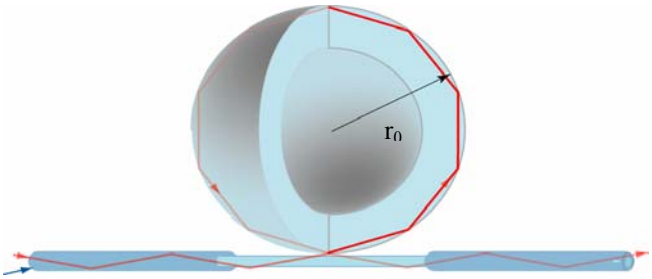

Figure 2: Optical path in the fiber and a coupled hollow microsphere

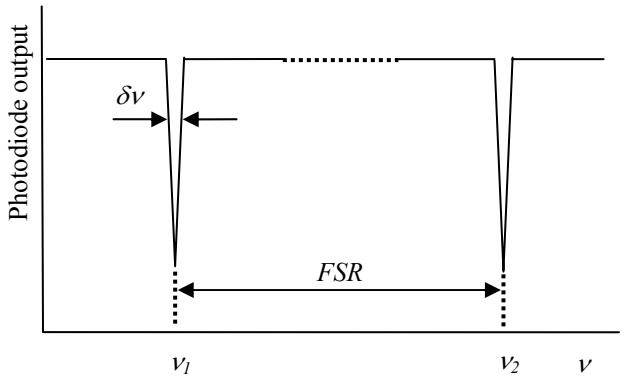

Figure 3: Transmission spectrum

The WGM technology belongs in the broader class of micro-optical mechanical systems (MOMS). But the principle of the WGM-based sensors provides a considerably finer resolution than any of the other methods in this class including frequency selective fiber-based Fabry-Perot interferometers [6] and Fiber-Bragg gratings. In their application as temperature, pressure (or force) sensors, the Fabry-Perot and Bragg grating techniques rely on the deflection of the optical beam to convert any change in a mechanical attribute of a structure (for example, a tip displacement) into the resonance frequency shift. This requires a precise alignment of a laser beam at the micro-fabricated mechanical system, and the use of an external photo-detector array for detecting the motion of the mechanical structure. Further, the amount of deflection/deformation required for the measurement is significantly larger that the change in the microsphere size or shape needed in the present technique. In the WGM sensing technology, mechanical deformations on the sub-nanometer scale can be detected and related to temperature, pressure or force causing it. Hence, it offers significant advantages over the currently available methods in measurement sensitivity and reliability as well as sensor ruggedness. Due to the optical attributes, the WGM-based sensors can be built with much smaller sensing element sizes than what is possible with the currently available methods. Hence, the compact and robust WGM micro-sensors can be incorporated into micro-optical sensor arrays for distributed measurements.

In addition to temperature and protein sensing, WGM-based microresonator-fiber coupling system have been suggested or demonstrated also in laser frequency locking and stabilization[7], high-Q microphotonic electro-optic modulator[8], tunable optical filters for optical network[9], thermo-optic switch based on WGM resonance tuning by temperature changes[10], and for optical sensing of biomolecules[3]. Here we extend the WGM-based technology to the new area of force sensing. The principal motivation of the current work is the development of wall shear sensors for aerospace applications based on the same principle. In this current paper we demonstrate the viability of the basic measurement principle.

II. Measurement Principle

The microsphere is, essentially, an optical cavity that acts as a sensing element. A change in size, shape or index of refraction of the microsphere imposed by the surrounding causes a shift in the WGM. This shift, in turn, can be related to the physical property of interest. Light with vacuum wavelength λ can be introduced into a dielectric microsphere of radius r_o and refractive index n, for example, by side-coupling it to a tapered optical fiber, as shown in Fig. 2. In the geometric optics limit, the WGMs in a microsphere are associated with optical ray paths such as the one shown in Fig.2. Light circles the interior of the sphere through total internal reflection and returns in phase. The condition for optical resonance is $2\pi r_0 n = l\lambda$ where l is an integer and a measure of the ratio of the roundtrip path to the wavelength. In terms of frequency, ν, this condition is $\nu = (c/2\pi r_0 n)l$ where c is the speed of light in vacuum. An incremental change in the index of refraction or radius of the sphere will result in a shift in the resonant frequency, therefore, any change in the physical condition of the surrounding that induces a change in index of refraction or radius of the microsphere can be sensed by monitoring the WGM shifts. The WGM are observed as

sharp dips in the transmission spectrum through the fiber as depicted in Fig 3. The observed linewidth, $\delta\nu$, is related to the quality factor, $Q = \nu/\delta\nu$. Smaller energy losses as the light circulates inside the sphere, lead to larger Q, with $Q \to \infty$ as the losses vanish. In order to utilize the full benefits of multiple photon circulation, a high value of Q must be attained. The principle advantage of WGM-based sensor concept is that WGMs of dielectric microspheres provide exceptionally large Q-factors. For fused silica microspheres with optical configurations shown in Fig.2, a Q value approaching the material loss limit of 10^{10} has been reported[1], and experimentally, Q values of up to 10^8 have been demonstrated experimentally.

Note that the observed linewidth determines the measurement resolution. If we consider $\delta\nu$ to be the smallest measurable WGM shift, using $Q = 10^8$, for a sphere of radius $r_0 \sim 100$ μm one obtains a "measurable" microsphere radius change of $\Delta r = 10^{-12}$ m. This length scale is smaller than the size of an atom. But it makes clear the extreme sensitivity that can be expected by measuring resonance line shifts. Consider a configuration shown in Fig 4 where the microsphere is subjected to a uniaxial stress. If we assume that the smallest measurable radius change is of the order of $\Delta r \sim 1$ nm, for a hollow, $r_0 = 100$ μm silica bead with 10μm wall thickness, a rough estimate gives a force resolution of $\Delta F < 10^{-3}$ N. If a polyester bead is used, the estimated resolution improves to $\Delta F \sim 10^{-5}$ N.

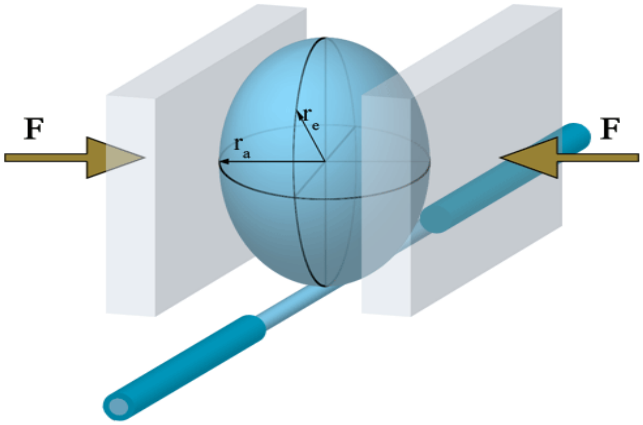

Figure 4: Microsphere with applied force.

The distance between two neighboring resonances, the free spectral range (*FSR*, as indicated in Fig. 3), is given by:

$$FSR = \frac{c}{2\pi n r_0}$$

While $\delta\nu$ defines the measurement resolution, *FSR* can be viewed as the measurement range. The ratio $F_r = FSR/\delta\nu$ is the finesse that indicates the dynamic range of measurement. For a microsphere with r_0=100 μm, $Q = 10^8$ and a laser wavelength of $\lambda \sim 0.6$ μm, $F_r \approx 60{,}000$. This value significantly exceeds finesse that is typical for a planar Fabry-Perot arrangement (F_r <100).

2.1. Optical Modes of a Uniform Dielectric Sphere

If several physical parameters are changing simultaneously, they may all contribute to the WGM shift. For example, both temperature and pressure induce a change in the WGM as both induce a size change (but not a shape distortion). However, the temperature change also induces a strong perturbation in the index of refraction in addition to the radius change[2]. Therefore, precisely how these resonances behave with a change in a given physical parameter is important in building sensors for specific applications.

For the range of practical interest covering microsphere radii of 5μm ≤ r ≤ 200μm, with laser wavelength $\lambda \sim 1$ μm (corresponding to 30 ≤ l ≤ 1200) one needs to reach beyond the geometric optics approximation and describe the resonances in terms of electromagnetic modes. The solution to Maxwell's equation for sphere provides three integer sets: n, l and m. The first quantum number, n, gives the number of nodes of the intensity distribution in radial direction. The orbital (or circumferential) quantum number, l, as described earlier, is approximately the number of wavelengths packed along the circumference of the resonator traveling along the equatorial belt of the sphere, and m is the azimuthal order number. For any value of l, m varies as $|m| \le l$. For the equatorial mode, $m = l$. In a perfect sphere with uniform index of refraction, all m modes have the same resonant wavelength as the mode with $m = l$. Therefore, for a perfect sphere, the transmission spectrum looks like that depicted in Fig 3, with only the l modes present. Any deviation from the spherical shape, however, will result in shifts of the m modes which will appear as additional dips in the transmission spectrum, which is typically the case for actual spectra.

2.2. Perturbations to Optical Modes

A first approximation of the shift in WGM caused by an outside perturbation is given by

$$\frac{\Delta\nu}{\nu_0} = -\frac{\Delta r}{r} - \frac{\Delta n}{n} - \frac{\Delta S}{S}$$

The first term on the right hand side represents a uniform expansion/compression of the microsphere by an amount Δr, whereas the second is the change of refractive index by an amount Δn. The last term describes the effect of shape distortion of the microsphere equator in terms of the eccentricity-induced round-trip path change by an amount, ΔS. Note that the undisturbed equatorial circumference is given by $S=2\pi r_0$.

The relative contribution of each term depends on the physical origin of the perturbation. The simplest effect is the pressure effect leading to a uniform expansion or compression. On the other hand, a temperature perturbation results in a change both in the radius and the refractive index. The WGM shift than is connected to the temperature change through $\frac{\Delta\nu}{\nu} = -\frac{\Delta r}{r} - \frac{\Delta n}{n} = (\alpha+\beta)\Delta T$, where α is the thermal expansion coefficient and β is the thermal coefficient for refractive index.

The principle of a WGM-based temperature sensor has recently been demonstrated[2]. For this, a setup similar

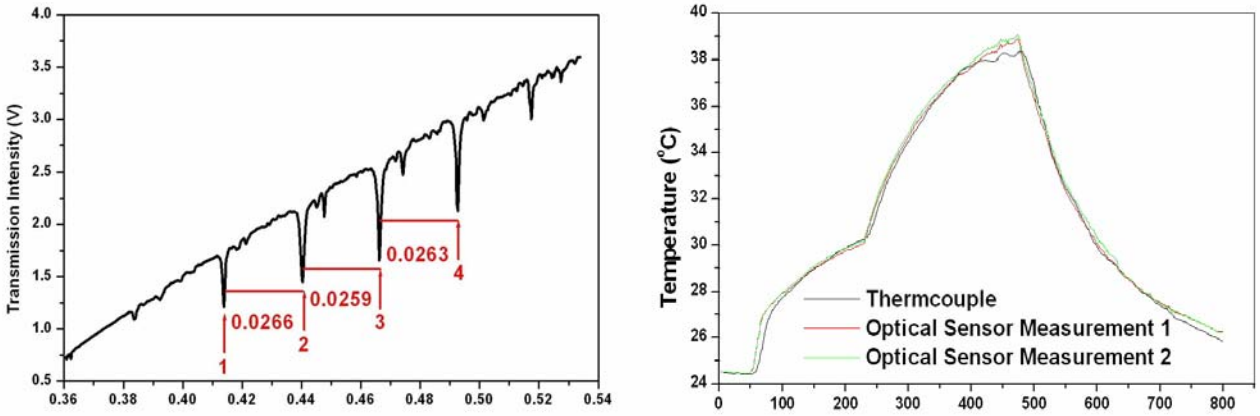

Figure 5: Typical transmission spectrum (left) and result (right) for a WGM temperature sensor (from [2]).

to that shown schematically in Fig. 1 was used. The sensing system which included a microsphere (whose diameter ranged between 150 and 400 μm) and a portion of the fiber etched to a diameter of about 4-5 μm was placed in a test cell which was either filled with water or air. Typical raw transmission spectra and comparison of temperatures measured by a WGM sensor and a thermocouple are shown in Fig 5. Note that the raw spectra shown is not normalized to remove the laser output power change with wavelength.

2.3. Mode Shift Due to Stress in Polar Direction

If anisotropic stress (such as in Fig 4) is applied to the microsphere, both the index of refraction perturbation term $\Delta n/n$ and the eccentricity term $\Delta S/S$ are likely to be at play. When the sphere is compressed, the sign of the latter term is positive. The sign of the term $\Delta n/n$ depends on whether the mechanical stress is positive or negative (tension or compression). Force tuning of WGMs was demonstrated earlier by mechanical compression of a fiber-coupled silica microsphere between piezo-activated pads[11]. Unfortunately, the force induced by the pads has not been measured in this study and the force-WGM shift relationship, therefore, is not available. The induced distortion of the microsphere shape removes the degeneracy of the $(2l + 1)$ multiplets and results in different frequencies for different m's for each value of l. The analytical modeling of the effect of anisotropic stress-induced deformation of the microsphere on the WGM resonances is a complex task. Below, we discuss only one specific case that is of importance to the force

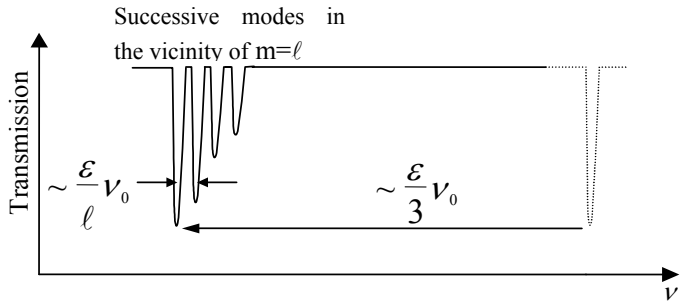

Figure 6. Effect of unipolar stress on microsphere resonance.

sensor discussed in this paper: unidirectional stress application resulting in the deformation of the sphere into a spheroid (an ellipsoid of revolution). (The following discussion does not take into account the possible effect of stress-induced changes in the index of refraction. In order to accurately factor in this effect, a detailed solid modeling analysis that provides not only the strain but also the stress distributions in the sphere is necessary. We are currently carrying out this task and plan to discuss the results in a future report).

When stress is applied along the polar axis (normal to the equatorial plane and the optical fiber direction, as shown in Fig. 4) the circumference in the equatorial plane ($l = m$) will expand as $S = S_0\left(1 - \varepsilon/3\right)$, and the largest elliptical circumference in the polar plane will contract as $S = S_0\left(1 + \varepsilon/6\right)$. Here $S = 2\pi r_0$ is the circumference of the original sphere and $\varepsilon = \dfrac{r_a - r_e}{r_0}$ is the eccentricity (r_e is the equatorial radius, r_a is the radius in polar direction which is the direction of applied force, as shown in Fig. 4, and r_0 is the radius the undisturbed sphere). The case of $\varepsilon < 0$ describes a compressed sphere (an oblate spheroid) and $\varepsilon > 0$ describes a stretched spheroid. For a Gaussian laser beam profile and if $m \approx l >> 1$ (for r_0=100 μm, n=1.5, and a laser wavelength of λ=0.6μm, $l \approx$1600), the frequency shift of the fundamental mode $l = m$ can be approximated by

$$\frac{\Delta\nu_{\ell,\ell=m}}{\nu} \approx \frac{\varepsilon}{3}$$

Similarly, the frequency splitting between two adjacent modes (l, m) and $(l, m-1)$ is $\dfrac{\Delta\nu_{\ell,m} - \Delta\nu_{\ell,m-1}}{\nu_0} \approx \dfrac{\varepsilon}{\ell}$.

Fig. 6 illustrates the mode shift and splitting due to unipolar stress on a microsphere. Note that the mode splitting due to the imposed eccentricity provides additional information that helps with sensor selectivity and can be used to separate stress from other effects caused by, for example, a simultaneous change in temperature. An additional piece of information that is of importance is the "direction" of the shift in the spectrum. A mode shift towards a higher frequency indicates that the sphere is being compressed whereas a shift to a lower frequency indicates that the sphere is decompressed. Therefore, as described in the forgoing, in addition to temperature and (isotropic) pressure, the technique can also be implemented as a force sensor, with very high sensitivity. In the present work, we present results using solid silica microspheres. As will be shown below, with the given setup we obtain a force sensitivity of ~ 0.01 N. By using softer dielectric sphere materials or using hollow glass particles, the sensitivity of the force sensor can be further improved.

III. Experimental Setup and Procedure

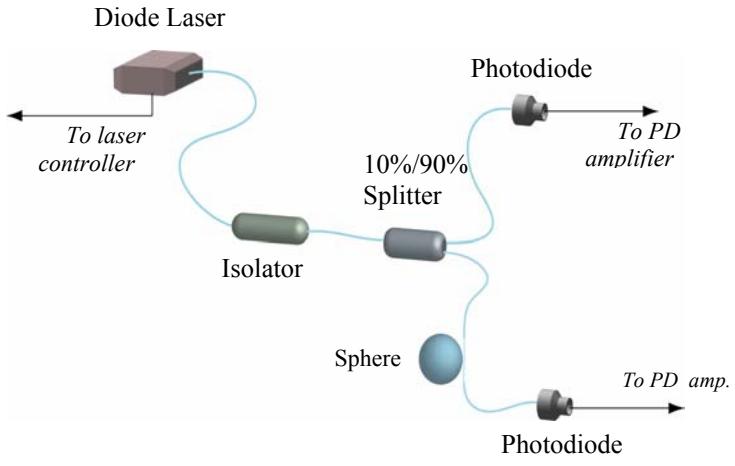

Figure 7: Schematic of the optical sensor setup

Figure 7 shows a schematic of the optical sensor setup. The output of a distributed feedback (DFB) laser diode (with a nominal wavelength of ~ 1312 nm) is coupled into a single mode optical fiber as shown. The diameter of the fiber core is ~ 9μm while the diameter with the cladding is ~ 130 μm. A portion of the laser light is extracted through a splitter to monitor its intensity as it is frequency tuned. A section of the other leg of the fiber is heated and stretched such that a taper is created with a minimum diameter of the order of 10μm. A microsphere, typically with a diameter of 200 - 400 μm, is brought into contact at a point in the stretched portion of the fiber thereby optically coupling the microsphere to the fiber. The overlapping evanescent fields of the fiber and the sphere

allow for the tunneling of light between the two elements. A photograph of the stretched portion of a fiber is shown in Fig 8. The microspheres are manufactured by heating one end of a short section of the optical fiber (including the cladding) using a microtorch. A photograph of a typical microsphere along with a portion of its stem is shown in Fig 9. The stem allows for the easy manipulation of the microsphere. The DFB laser is current tuned using a laser controller. The controller also keeps laser diode's temperature constant. The laser controller, in turn, is driven by a function generator which provides a saw tooth input to the controller. The output of the optical fiber, past the microsphere is coupled to a second photodiode (PD). The PD outputs as well as the function generator output are sampled using an A/D converter that is part of a personal computer (PC). The reference PD output is used to normalize the spectrum from the sensor fiber.

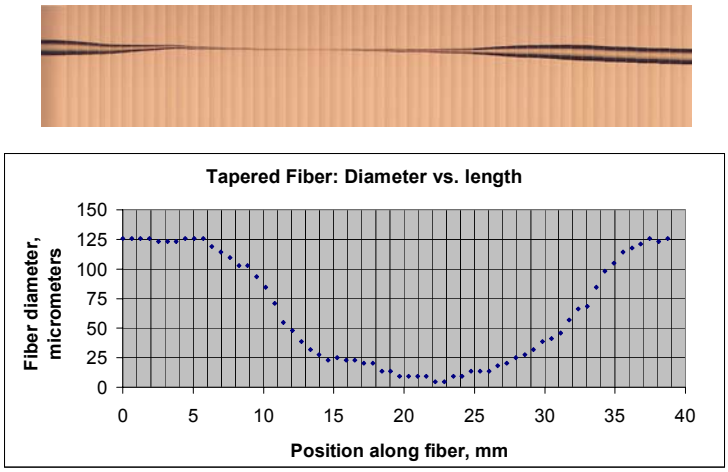

Figure 8: Typical stretched fiber section

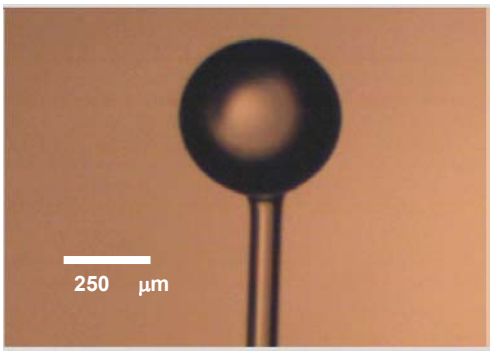

Figure 9: Photo of microsphere

The PC performs the scanning, data acquisition and analysis which includes the identification and monitoring of the shifts in the optical resonances (WGM). The force is exerted on the microsphere using two stainless steel pads that compress the microsphere along the polar direction. (The polar direction is that normal to the plane of light circulation in the sphere; Fig 4). As shown in Fig 10, one of the pads is driven by a micro-translation stage and is connected to a load cell that measures the force. The motion of the translation stage is also controlled by the PC.

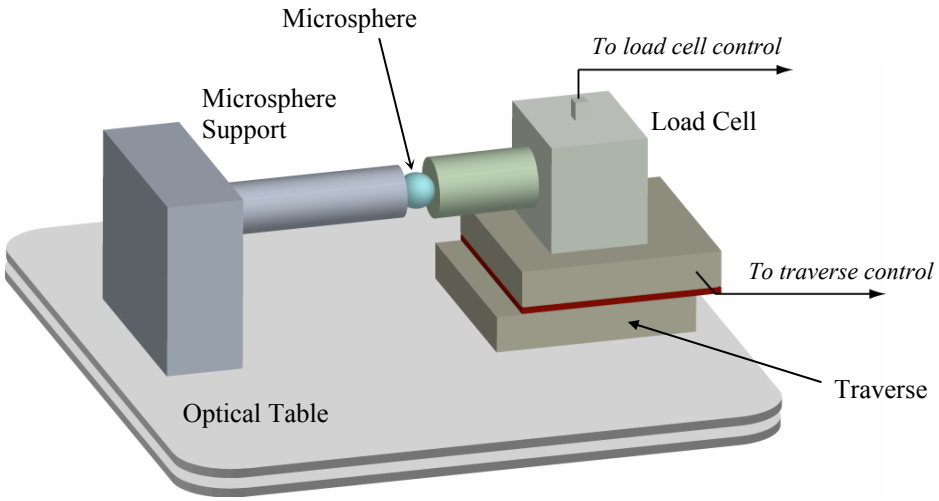

Figure 10: Microsphere compression setup

Figure 11 shows a photograph of the compression pads along with the microsphere and the optical fiber. A set of preliminary results with this setup is also shown in the figure. In this preliminary experiment, a microsphere of ~200 μm diameter is compressed by the pads as shown. On the right are six transmission spectra for the sensor. The top spectra is for that when there is no force applied to the microsphere (sensor). Each of the subsequent figures shows the same spectra with increasing force applied to the sensor. The applied force for the bottom spectra is approximately 0.5 N. As the applied force increases, the WGM indicated in the figure shifts in the positive direction (the resonant wavelength increases with increasing compression force). The figure demonstrates the capability of the approach for measurement of unidirectional force.

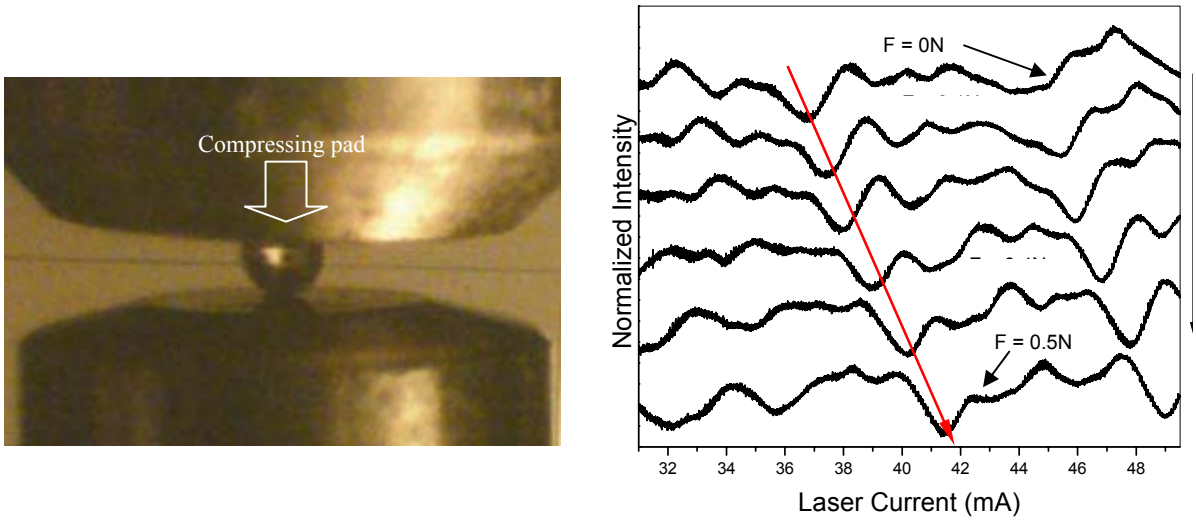

Figure 11: Effect of applied force. Photograph of the sensor and pads (left) and observed shift in WGM (right).

IV. Experimental Results

A series of experiments were carried out to investigate the dependence of WGM shifts on compression force applied to microsphere sensors using the setup shown in Fig 10. Figure 12 shows the WGM shifts for the complete

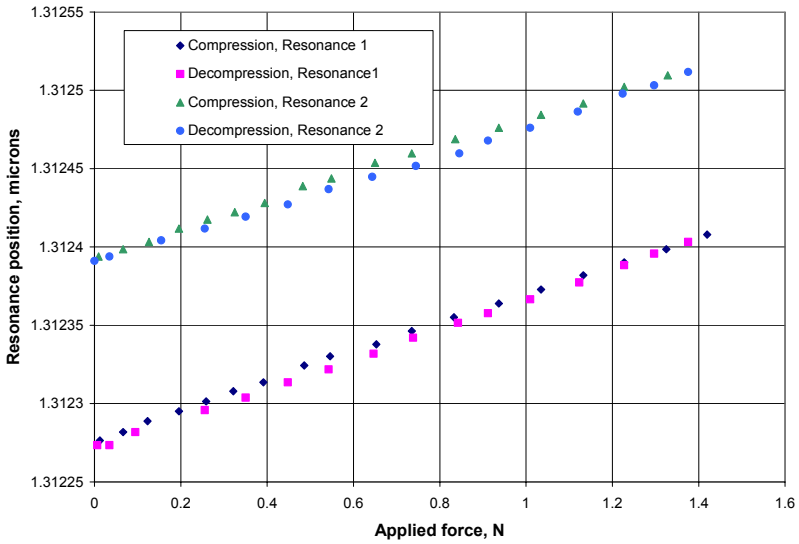

Figure 12: Study of hysteresis on resonance shifts

compression and decompression cycle. The sensor diameter for this preliminary experiment is ~ 350 μm with a modest Q-factor of the order of about 10^5. Two resonances dips, approximately 0.12 nm apart, are followed within the scanning range of the laser. For each resonance, the compression and decompression curves are essentially identical indicating that there is no measurement hysteresis. Note that in all the force measurements discussed here, the temperature of the environment surrounding the sensor is kept constant in order to avoid the additional effect temperature on resonance shifts.

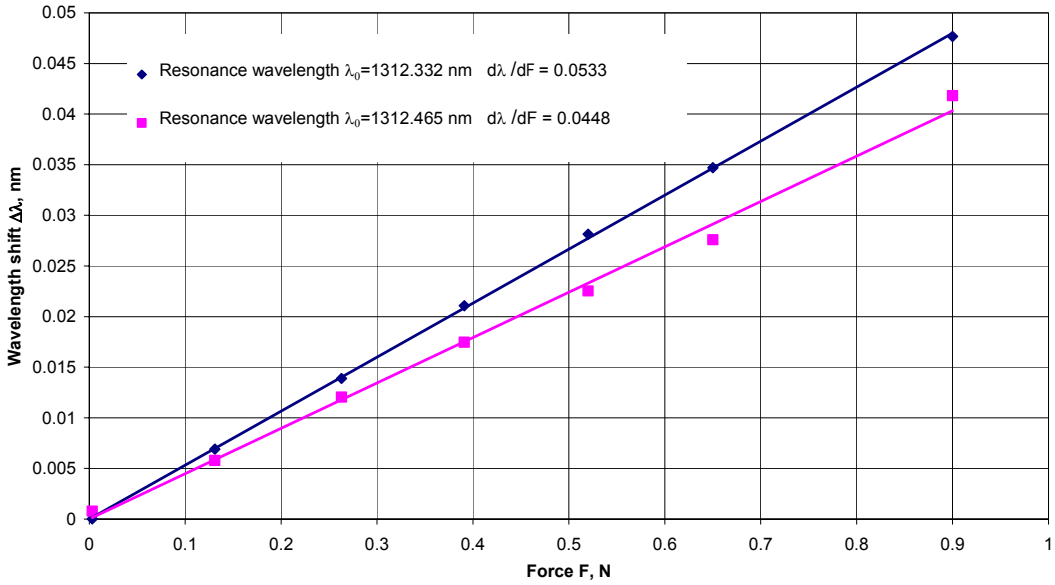

Figure 13: Resonance shift versus force (10 Hz scan rate)

The effect of force on resonant wavelength shift is shown in Fig 13. In this measurement, a 340 μm microsphere is used. The diode laser is scanned in a 0.18 nm wavelength range with a scanning repetition rate of 10 Hz. Again the two distinct resonances within the transmission spectrum are tracked in the figure. The resonant wavelengths, λ_0, corresponding to zero loading are indicated in the figure. Throughout these measurements the resonance locations in the spectrum are determined by fitting each dip to a function and selecting the minimum value of this function. Figure 13 shows that the dependence of the wavelength shift on the force is linear in the force range considered. The quality factor for this measurement is determined to be $Q \approx 3.78 \times 10^6$, indicating a measurement sensitivity better than 10^{-2} N.

An interesting feature observed in Fig. 13 is that the two resonances have slightly different slopes. The slope for the resonance with the shorter wavelength is larger and the relative difference between the two slopes is approximately 15%. In general, several factors could contribute to the observed difference in the slopes. For example, although different circumferential modes (l, $l+1$, $l+2$, etc.) would be expected to have the same $d\lambda/dF$ slopes, different azimuthal (m) modes for a given l mode could potentially yield different slopes due to the eccentricity introduced by the compression of the sphere in the polar direction. Another likely cause of the observed difference in slopes is due to the possible variation of the laser diode temperature through each scan. The laser frequency is scanned by varying the electrical current supplied to it. Although the laser temperature is stabilized by a Peltier-type control loop, the rapid ramping of the current to the laser could result in small temperature variations within each scan. The laser calibration curves of Fig. 14 shows the strong dependence of the wavelength on laser temperature. The calibrations are carried out using a

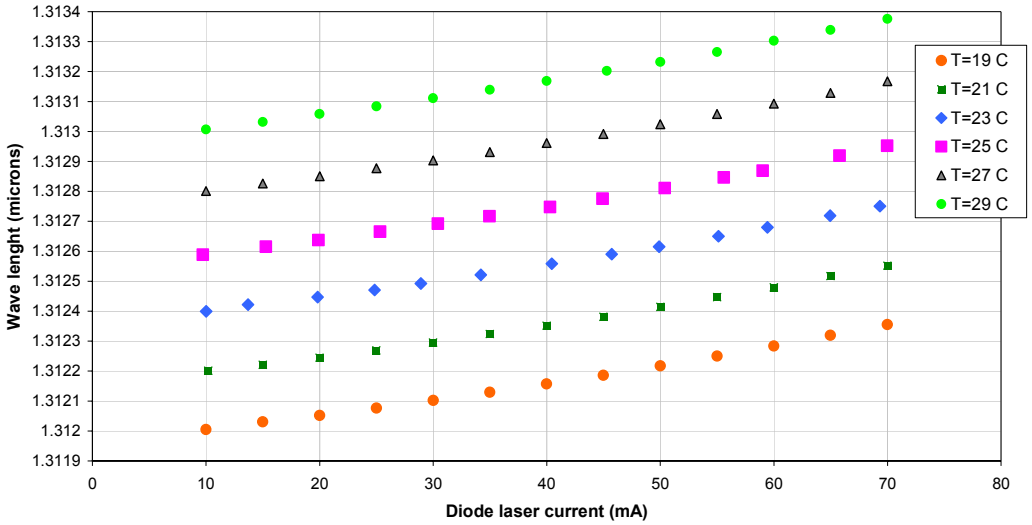

Figure 14: Calibration curves for the DFB laser

laser wavemeter and at six different laser temperatures as shown. Figure 14 indicates that, for example, a 0.1 ^{o}C change in the laser temperature during the scan would result in an unintended laser wavelength shift of ~ 0.01nm. In Fig 13, the laser frequency is tuned by ramping up the current by an amount of 35 mA over a period of approximately 100 ms. At the end of the ramp, the current suddenly drops back to the initial value. The same cycle is repeated over with at the rate of 10 Hz. It is possible that the temperature controller may not be able to respond fast enough to the cyclic, unsteady heat addition to keep the temperature of the laser constant and small temperature variations may result. If the scan rate is reduced, the temperature variations through each scanning cycle should also be reduced leading to smaller variations in the $d\lambda/dF$ from different resonances. Figure 15 tends to confirms this.

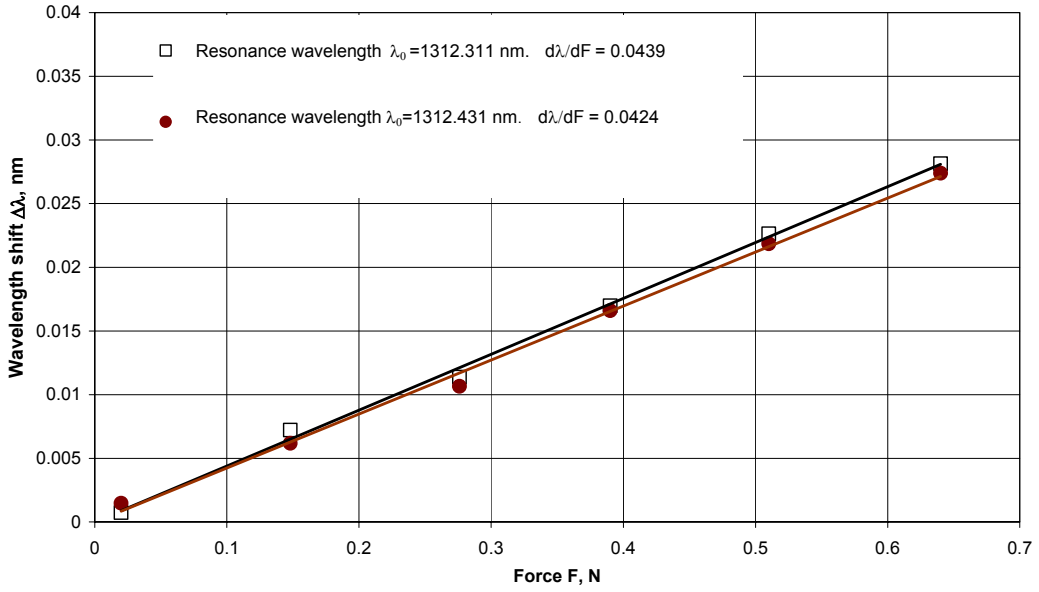

Figure 13: Resonance shift versus force (0.5 Hz scan rate)

The figure shows the shift in two distinct resonances as the force is applied to the sphere but this time at a much smaller scan rate of 0.5 Hz. Again, λ_0 represents the initial resonant wavelength for each mode before force is applied. By scanning the laser slowly, the relative difference in the two slopes is reduced to less than 3.5%.

Although reducing the scan rate of the laser is an option to minimize calibration (gain) errors in the micro-optical force sensor, in the future we will investigate additional approaches to reduce laser temperature variation effects.

Our longer term goal is to design and implement a sensor that provides information that is well resolved not only in space but also in time which will require faster laser scanning and data analysis rates.

V. Conclusions

A novel micro-optical force sensor that is based on the morphology dependent shifts optical modes (WGMs) of silica microspheres is demonstrated in this work. The diameter of the microspheres ranged between 200 and 350 μm. In order to excite the optical modes of a sphere, tuneable laser light is coupled into it via a single mode optical fiber. The optical coupling between the fiber and the sphere is facilitated by heating and stretching a small section of the fiber. Once the microsphere is brought into contact with the stretched section of the fiber, WGMs of the spheres were observed in the transmission spectrum through the fiber. The diameter of the fiber in the coupling region varied between 9 and 15 μm. In some of the measurements, Q-factors in excess of 10^6 were obtained. These Q values and the experimental data show that force measurements with resolutions better than 10^{-2} N are possible using solid silica spheres. The results show a linear relationship between the WGM shifts and applied force in the range 0 - 1 N. Both strain (shape change) and stress can potentially induce WGM shifts. The strain effect is due to the change in the round trip distance light travels inside the sphere. The effect of normal stress in the glass is through the change in the index of refraction. For fused silica, tension stress reduces the index of refraction while compression stress increases it. Hence, since the stress around the equatorial belt of sphere is expected to be tension, the corresponding index of refraction is expected to become smaller leading to WGM shifts towards shorter wavelengths as force is applied. However, the experiments show that increasing uniaxial force applied in the polar direction leads to increased mode wavelengths indicating that the WGM shifts are dominated by the strain effect. Future work includes detailed numerical solid modeling in order to determine stress and strain distributions in the sphere coupled with optical calculations to fully analyze the experimental result and help in the development of micro-optical wall shear stress sensor applicable to a wide range of aerodynamic flows.

Acknowledgments

The support by the National Science Foundation through grant no. CTS-0502421 is gratefully acknowledged.

References

[1] Gorodetsky, M. L., Savchenkov, A.A. and V.S. Ilchenko. "Ultimate Q of optical microsphere resonators." *Optics Letters* Vol. 21n No 7, 1996. pp. 453-455.

[2] Guan, G., Arnold, S. and Otugen, V., "Temperature Measurements Using a Micro-Optical Sensor Based on Whispering Gallery Modes", *Infotech@ Aerospace Conference*, September 26-29, Arlington, VA

[3] Vollmer, F., Braun, D., Libchaber, A., Khoshsima, M., Teraoka, I. and Arnold, S. "Protein Detection by Optical Shift of a Resonant Microcavity", *Applied Physics Letters* Vol. 80, 2002, pp. 4057–4059.

[4] Arnold, S., Khoshsima, M., Teraoka, I., Holler, S. and Vollmer, F. "Shift of Whispering-Gallery Modes in Microspheres by Protein Adsorption", *Optics Letters*, Vol. 28, No. 4, 2003, pp. 272-274.

[5] Teraoka, I., Arnold, S. and Vollmer, F. "Perturbation Approach to Resonance Shifts of Whispering-Gallery Modes in a Dielectric Microsphere as a Probe of a Surrounding Medium", *JOSA B*, Vol. 20, No. 9, 2003, pp. 1937-1946.

[6] Tseng, F-G and Lin, C-J, "Polymer MEMS-Based Fabry-Perot Shear Stress Sensor", *IEEE Sensors Journal*, Vol. 3, No. 6, 2003, pp. 812-817.

[7] Griffel, G., et al., "Morphology-dependent resonances of a microsphere-optical fiber system", *Optics Letters*, Vol. 2, No. 10, 1996, pp. 695-697.

[8] Cohen, D.A., Hossein-Zadeh, M. and Levi, A.F.J., "High-Q Microphotonic Electro-optic Modulator", *Solid-State Electronics*, Vol. 45, No. 9, 2001, pp. 1577-1589.

[9] Savchenkov, A.A., et al., "Tunable Filter Based on Whispering Gallery Modes", *Electronics Letters*, Vol. 39, No. 4, 2003, pp. 389-391.

[10] Tapalian, H.C., Laine, J.P. and Lane, P.A., "Thermooptical Switches Using Coated Microsphere Resonators", *IEEE Photonics Technology Letters*. Vol. 14, No. 8, 2002, pp. 1118-1120.

[11] Ilchenko, V.S., Volikov. P.S. Velichansky, V.L., Treussart, F, Lefevre-Sequin, V., Raimond, J-M., and Haroche, S., "Strain-Tunable High-Q Optical Microsphere Resonator", *Optics Communications*, Vol. 145, January 1998, pp. 86-90.